Magnetism and charge ordering in $Pr_{0.5}Ca_xSr_{0.5-x}MnO_3$ ($x=0.09$ and 0.5)

Z. Jirák
Institute of Physics of ASCR, Na Slovance 2, 18221 Prague 8, Czech Republic

F. Damay, M. Hervieu, C. Martin, and B. Raveau
Laboratoire CRISMAT, URA CNRS 1318, ISMRa, Bd du Maréchal Juin, 14050 Caen, France

G. André and F. Bourée
Laboratoire Léon Brillouin, CEA/Saclay, 91191 Gif-sur-Yvette, France
(Received 28 April 1999; revised manuscript received 30 June 1999)

The structural and magnetic transitions in two Mn^{3+}/Mn^{4+}(1:1) systems have been investigated using neutron diffraction and electron microscopy. In $Pr_{0.5}Ca_{0.5}MnO_3$, the charge and orbital order develops in the paramagnetic phase of *Pnma* symmetry below $T_{co}=250$ K through a sequence of incommensurate configurations. The ordering process is accomplished at $T_N=170$ K where the charge-exchange–(CE) type antiferromagnetism sets in. Despite the superstructure, the tilt pattern of *Pnma* type is preserved down to the lowest temperatures. The second compound, $Pr_{0.5}Ca_{0.09}Sr_{0.41}MnO_3$, is ferromagnetic below $T_C=240$ K. The charge ordering occurs at $T_N=180$ K and is accompanied by the onset of the CE antiferromagnetism. The transition is associated with a change of the tilt pattern from $I4/mcm$ to *Imma* type. The low-temperature phase is commensurate both in the structural and magnetic sense. It is argued that the main energy gain of the charge ordering in Mn^{3+}/Mn^{4+} (1:1) perovskites results from electron-exchange interactions favored by the e_g orbital polarization. The onset of the incommensurate configurations can be understood supposing the existence of a soft lattice mode in which the electron transfer (charge-density wave) is correlated with dynamics of e_g orbitals.

I. INTRODUCTION

The recent investigation of the $Pr_{0.5}Ca_xSr_{0.5-x}MnO_3$ series has shown an important role of size of the *A* cations upon the crystallographic and magnetic ordering phenomena.[1] Taking also into account other $Ln_{0.5}A_{0.5}MnO_3$ perovskites, one finds a general behavior. The system with largest cations, $La_{0.5}Sr_{0.5}MnO_3$, is pseudocubic with a small rhombohedral or tetragonal distortion. These structures involve rotations of the MnO_6 octahedra around the unique axis, which results in a deviation of the Mn-O-Mn angles from the ideal 180°. For the rhombohedral modification of $La_{0.5}Sr_{0.5}MnO_3$, the actual angles can be estimated from lattice parameters to 171°–172°.[2] In the tetragonal modification of the same compound, there are two distinct Mn-O-Mn angles, one of 180° along the *c* axis and two in-plane angles that were determined to be 170°. The isostructural $Pr_{0.5}Sr_{0.5}MnO_3$ with decreased average *A* cation exhibits the Mn-O-Mn in-plane angles of 165°.[3] Futher lowering of *A* cation size by calcium substitution in the $Pr_{0.5}Ca_xSr_{0.5-x}MnO_3$ series results in orthorhombic structures that are characterized with another tilt pattern of the MnO_6 octahedra called ''buckling.'' The space-group symmetry is *Imma* in a narrow interval close to the orthorhombic-tetragonal boundary at $x\sim0.09$ and it is *Pnma* for $x>0.1$. The Mn-O-Mn angles are rather uniform and range from 163°–168° for the $x=0.09$ sample already reported[4] to about 158° for $x=0.5$. The angles are further decreased with the substitution of praseodymium by smaller rare-earth cations. It is worth mentioning that among the *Pnma* systems studied we observed an extreme orthorhombic deformation for the $Y_{0.5}Ca_{0.5}MnO_3$ compound and determined the Mn-O-Mn angles to be 151°.

The change of the octahedral tilt with decreasing *A* cation size is reflected in the strength of ferromagnetic (double-exchange) interactions. The maximum $T_C=360$ K is achieved for the rhombohedral $La_{0.5}Sr_{0.5}MnO_3$ where the ferromagnetism remains stable down to the lowest temperatures. The tetragonal $La_{0.5}Sr_{0.5}MnO_3$ and $Pr_{0.5}Sr_{0.5}MnO_3$ order ferromagnetically at considerably lower temperatures, $T_C=310$ and 265 K, respectively. When lowering the temperature, these compounds undergo a second transition to the *A*-type antiferromagnetism. The antiferromagnetic ground state in that case is associated with orbital $d_{x^2-y^2}$ polarization of itinerant e_g electrons. On the other hand, the orthorhombic systems $Pr_{0.5}Ca_xSr_{0.5-x}MnO_3$ for $x\geqslant0.09$ ($T_N\sim170$–180 K), as well as the mentioned compound $Y_{0.5}Ca_{0.5}MnO_3$($T_N=110$ K), all possess an antiferromagnetic ground state of the charge-exchange–(CE) type, which is indicative for the concomitant 1:1 Mn^{3+}/Mn^{4+} charge and $d_{3z^2-r^2}$ orbital order.

The temperature behavior in the $Pr_{0.5}Ca_xSr_{0.5-x}MnO_3$ series varies with different calcium doping, despite the same CE-type ground state. In the region $0.09\leqslant x<0.25$ there is always a ferromagnetic domain at intermediate temperatures, which precedes the onset of charge order and antiferromagnetism at $T_{co}=T_N$. For $x>0.25$, the charge ordering occurs in the paramagnetic state well above T_N. It is important, namely from the point of view of magnetoresistive properties, that the ferromagnetism does not vanish totally and it persists as a parasitic phase or dispersed clusters that may

grow and become magnetically polarized by an action of the external field. The amount of the ferromagnetic impurities in the charge ordered paramagnetic phase diminishes quickly for larger x, i.e., towards pure $Pr_{0.5}Ca_{0.5}MnO_3$.[5]

The present paper is focused to a detailed neutronographic and electron-microscopy investigation of the 1:1 Mn^{3+}/Mn^{4+} order and CE-type antiferromagnetism in two members of the $Pr_{0.5}Ca_xSr_{0.5-x}MnO_3$ series, $x=0.09$ and 0.5.

II. EXPERIMENT

Samples $Pr_{0.5}Ca_{0.5}MnO_3$ and $Pr_{0.5}Ca_{0.09}Sr_{0.41}MnO_3$ were prepared by thoroughly mixing Pr_6O_{11}, $SrCO_3$, CaO, and MnO_2 in stoichiometric proportions. The mixture was first heated at 950 °C, two times, with intermediate grinding, to achieve decarbonation. Powder was pressed into the form of pellets under 1 ton/cm^2 and sintered at 1500 °C for 12 h in air. The samples were then cooled at 5 °C min^{-1} down to 800°C and finally quenched to room temperature. Neutron experiments were carried out at the LLB (Saclay, France) on the G41 diffractometer using a wavelength $\lambda=2.4266$ Å to determine the temperature evolution of nuclear and magnetic structures. Samples were first cooled down to helium temperature and patterns were recorded over an angular range $17°<2\theta<97°$ by warming from 2 K to room temperature. Additional patterns using the high-resolution diffractometer $3T2$ with a wavelength $\lambda=1.227$ Å were registered in the range $6°<2\theta<125°$ at selected temperatures, 292 K, 10 K, and at one intermediate temperature (185 K for $Pr_{0.5}Ca_{0.5}MnO_3$ and 200 K for $Pr_{0.5}Ca_{0.09}Sr_{0.41}MnO_3$), in order to get more information on the nuclear structure. The diffraction patterns were analyzed with the Rietveld method using the FULLPROF program (version 3.1c Jan96-LLB-JRC).

Numerous crystallites of samples used for the neutron-diffraction study were characterized using electron-diffraction and high-resolution electron-microscopy. The diffraction study versus temperature and the bright/dark field imaging were carried out with a JEOL 2010 electron microscope using a double-tilt cooling sample holder. For most of the experiments, the temperature was firstly stabilized at 92 K and then slowly increased to 300 K, waiting for the temperature stabilization before each recording. Resistivity measurements were performed, using a four-probe method on sintered bars with $2\times2\times10$-mm^3 dimensions, from room temperature down to 5 K. The ac susceptibility measurements were performed with a Lake Shore AC 7000 susceptometer. The sample was first zero-field cooled to 5 K and the curve was then registered with $h_{ac}=10$ Oe and $f=33$ Hz.

III. RESULTS

The structural parameters determined by neutron diffraction at 292 K are summarized in Table I. In accordance with the earlier finding, the $Pr_{0.5}Ca_{0.5}MnO_3$ sample possesses the *Pnma* structure whereas $Pr_{0.5}Ca_{0.09}Sr_{0.41}MnO_3$ shows a simpler tilt pattern resulting in a body-centered symmetry *Imma*. The temperature sequence of phases in $Pr_{0.5}Ca_{0.09}Sr_{0.41}MnO3$ is illustrated in Fig. 1 and is complemented with the susceptibility and resistivity measurements. More complete data are reported in Ref. 4. We note that, upon cooling, there is a two-phase region between 260 and 240 K where the high-temperature orthorhombic *Imma* phase coexists with a new phase of the tetragonal $I4/mcm$ symmetry. The transition is accomplished at $T_C=240$ K where the ferromagnetic order sets in. Lattice parameters at 200 K, $a=5.3854(1)$ Å, $c=7.7850(2)$ Å indicate a marked tetragonal distortion of the perovskite structure with ratio $c/a\sqrt{2}=1.022$. The observed ferromagnetic moments of 2.17(5) μ_B are oriented along the c direction.

In a very narrow interval around 180 K, the ferromagnetic phase of the $I4/mcm$ symmetry is transformed to the CE antiferromagnetic structure of the orthorhombic *Imma* type. The room-temperature tilt pattern is thus reentered. The parameters of the *Imma* subcell are $a=5.4442(2)$ Å, $b=7.5145(2)$ Å, and $c=5.5131(2)$ Å at 10 K. Compared with the room-temperature data, one observes a marked pseudotetragonal compression along the b axis, which is characteristic for all Mn^{3+}/Mn^{4+} (1:1) ordered phases. The charge and orbital ordering below $T_{co}=T_N=180$ K is associated with the commensurate wave vector $\vec{q}=1/2,0,0$ and results in a doubled cell of the orthorhombic symmetry *Pmmn*. The wave vector is linked to the a axis and is thus coupled to the octahedral tilt in a unique way, similar to what was reported by Radaelli *et al.* for $La_{0.5}Ca_{0.5}MnO_3$.[6] The antiferromagnetic order of the CE type involves further doubling in the c direction. The ordered moments amount to 3.18(9) μ_B and 2.83(8) μ_B for Mn^{3+} and Mn^{4+} sites, respectively, and are aligned along the c axis in the basal (pseudotetragonal) plane.

The results of the unconstrained refinement of the low-temperature phase in $Pr_{0.5}Ca_{0.09}Sr_{0.41}MnO_3$ are shown in Figs. 2 and 3. It is seen that the structure exhibits two distinct manganese octahedra. The first one is tetragonally elongated, which is indicative for the $d_{3z^2-r^2}$ polarization of the e_g orbitals. Consequently, the site can be identified with Mn^{3+}. The distortion is, however, only half of that observed in $PrMnO_3$.[7] The second octahedron is nearly regular but the Mn^{4+} cation is located 0.057 Å off center, approaching three of its oxygen ligands. The structural modulation associated with the charge ordering involves alternative displacements of the Mn^{4+} octahedra along the c axis (Fig. 3). These displacements are mainly responsible for the occurrence of superstructure lines in diffraction experiments.

The temperature behavior of the second compound under study, $Pr_{0.5}Ca_{0.5}MnO_3$, is illustrated in Fig. 4. The sample exhibits a charge ordering transition at $T_{co}=250$ K, without change of the *Pnma* tilt pattern. The pseudotetragonal deformation develops very slowly and saturates at much lower temperature close to $T_N=170$ K where the antiferromagnetic CE structure sets in. Similar to the lanthanum analog,[6] the ordering is associated with an incommensurate modulation with wave vector $\vec{q}=1/2\text{-}\varepsilon,0,0$ where ε varies with temperature and approaches zero in the antiferromagnetic state. The data derived from the observed splitting of superstructure spots in the electron-diffraction experiments are summarized in Fig. 5. It is seen that there is some residual incommensurity even below T_N, which is actually given by $\varepsilon\sim0.02$. When increasing the temperature, the ε value increases in a step-like manner and finally achieves $\varepsilon\sim0.15$

TABLE I. Structural parameters, selected interatomic distances, and angles at room temperature.

Sample	$Pr_{0.5}Ca_{0.5}MnO_3$	$Pr_{0.5}Ca_{0.09}Sr_{0.41}MnO_3$
Space group	*Pnma*	*Imma*
a(Å)	5.4042(2)	5.4312(2)
b(Å)	7.6064(2)	7.6250(3)
c(Å)	5.3949(1)	5.4729(2)
Volume (Å^3)	221.77	226.65
Pr,Ca,Sr	*site* 4*c*	*site* 4*e*
x	0.0304(3)	0
y	0.25	0.25
z	−0.0061(6)	0.0011(3)
B(Å^2)	0.72(2)	0.74(2)
Mn	*site* 4*b*	*site* 4*b*
x	0	0
y	0	0
z	0.5	0.5
B(Å^2)	0.34(2)	0.21(2)
O(1)	*site* 4*c*	*site* 4*e*
x	0.4888(3)	0
y	0.25	0.25
z	0.0674(3)	0.5525(3)
B(Å^2)	0.68(3)	0.94(3)
O(2)	*site* 8*d*	*site* 8*g*
x	0.2844(2)	0.25
y	0.0348(1)	−0.0267
z	−0.2842(2)	0.75
B(Å^2)	0.70(1)	1.18(2)
R_{wp}(%)	5.37	6.73
χ^2(%)	1.41	2.32
Mn-O(1)(Å)	1.937(0)(2×)	1.928(0)(2×)
Mn-O(2)(Å)	1.944(1)(2×)	1.938(0)(4×)
	1.946(1)(2×)	
O(1)-Mn-O(2)(°)	89.74(9)	89.92(6)
O(1)-Mn-O(2)(°)	89.81(9)	89.92(6)
O(2)-Mn-O(2)(°)	89.03(8)	88.94(5)
Mn-O(1)-Mn(°)	158.07(14)	162.85(10)
Mn-O(2)-Mn(°)	157.92(11)	167.95(6)

just before the superstructure spots vanished at T_{co}. At cooling, the sample showed no apparent hysteresis.

In the neutron-diffraction patterns of $Pr_{0.5}Ca_{0.5}MnO_3$, the charge ordering is manifested by the occurrence of additional nuclear lines and, below T_N, by magnetic peaks. Figure 6 shows the temperature evolution of nuclear satellites located near (1/2,2,2) at $2\theta = 68.7°$ in Fig. 6 (see also, $2\theta = 33.1°$ in Fig. 7). Other satellites are much weaker or obscured by main reflections, which makes determination of the modulation vector $\vec{q} = 1/2\text{-}\varepsilon,0,0$ difficult. Nevertheless, the fitting of the high-resolution neutron-diffraction pattern at 185 K by FULLPROF using so-called matching mode for nuclear satellites provided a value of $\varepsilon \sim 0.017(3)$, which was in good agreement with the electron-diffraction results.

Magnetic peaks are shown in detail in the lower panel of Fig. 7. It appears that line (1,1,1/2) is heavily broadened and some broadening can be detected also on other magnetic lines (h integer, k odd, l half-integer) that originate from the Mn^{3+} sites in the CE antiferromagnetic arrangement. On the other hand, the lines from the Mn^{4+} sublattice, e.g., (1/2,1,1/2) are narrow at all temperatures. As pointed out by Radaelli *et al.*[6] for $La_{0.5}Ca_{0.5}MnO_3$, the different behavior of these two sets of magnetic lines indicates that the structural modulation does not represent a homogeneous wave. Instead, it consists of domains of commensurate order that are pseudoperiodically separated with orbital order defects (*discommensurations*) where moments on the Mn^{3+} sublattice are reversed, while ordering of the Mn^{4+} spins is not affected. The temperature evolution of the line (1,1,1/2) in Fig. 8 shows that the characteristic broadening remains constant up to ~150 K, then it decreases gradually up to $T_N = 170$ K where magnetic lines disappeared. Such behavior suggests that above 150 K the magnetic order survived only in a discommensuration-free part of our $Pr_{0.5}Ca_{0.5}MnO_3$ sample, which can be estimated to about 10%.

Structural determination of the charge ordered phase $Pr_{0.5}Ca_{0.5}MnO_3$ was attempted using the high-resolution neutron-diffraction pattern at 10 K, which is shown in Fig. 7.

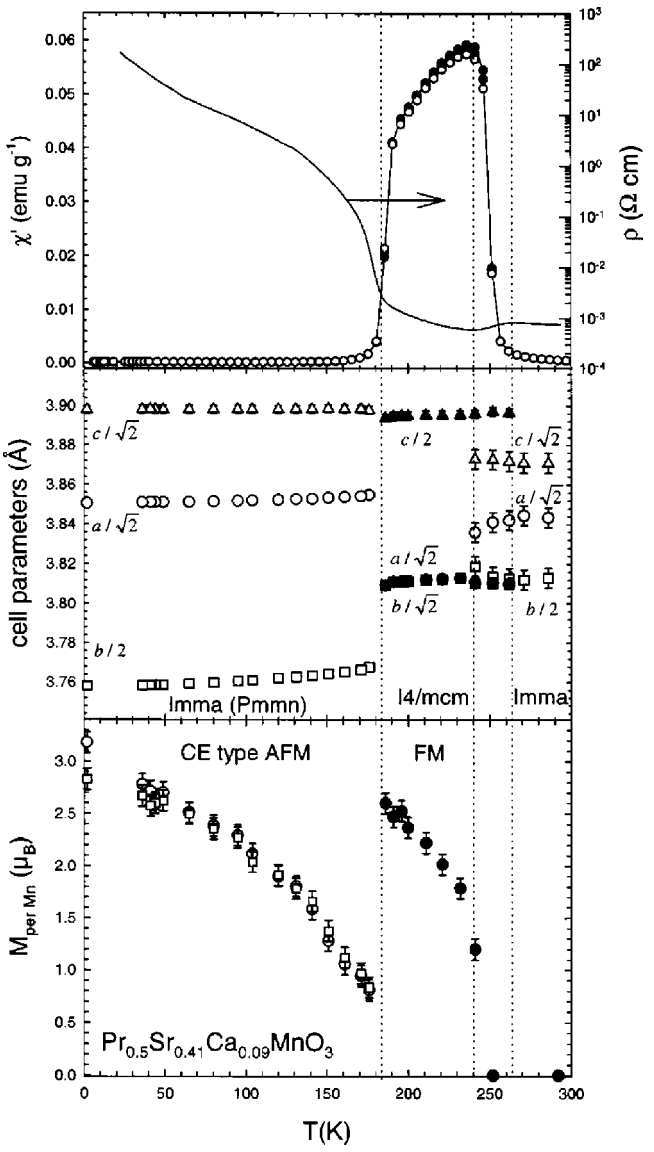

FIG. 1. $Pr_{0.5}Ca_{0.09}Sr_{0.41}MnO_3$: temperature dependence of (a) the susceptibility (left axis), the resistivity (right axis), (b) the lattice parameters, and (c) the ferromagnetic and the antiferromagnetic components. The dotted lines delimit the different states exhibited by this compound.

Analysis of magnetic peaks within the discommensuration model resulted in the modulation vector $\vec{q}=1/2\text{-}\varepsilon,0,0$ with $\varepsilon=0.016(1)$. Consequently, the final refinement of the magnetic structure was performed in a supercell 62 times enlarged in the *a* direction, which contained two discommensurations of the Radaelli type with spacing of about 170 Å. [The model is illustrated below in Fig. 10(c).] The observed asymmetrical intensity of left and right satellites at $2\theta \sim 17°$ was satisfactorily reproduced (see lower panel of Fig. 7) provided that the spacing of Mn sites along the *a* axis was larger in the commensurate domains than at the discommensuration boundaries. The extent of $Mn^{3+}O_6$ octahedral distortions and (correlated with them) $Mn^{4+}O_6$ displacements was found to be essentially the same as in the commensurate structure of $Pr_{0.5}Ca_{0.09}Sr_{0.41}MnO_3$.[4]

The lattice parameters of $Pr_{0.5}Ca_{0.5}MnO_3$ at 10 K were determined to $a=5.4357(2)$ Å, $b=7.4831(2)$ Å, $c=5.4335(2)$ Å with respect to the *Pnma* cell. The magnetic moments in the CE arrangement achieved values of 3.18(7) μ_B and 2.75(5) μ_B for the Mn^{3+} and Mn^{4+} sites, respectively. Similarly to some other *Pnma* manganites with the CE arrangement (see e.g., Ref. 6), we have observed an inclination of the Mn^{3+} spins to 35° from the *c* axis towards the *a* axis. The orientation of the Mn^{4+} spins could not be determined with certainty because of the pseudotetragonal metrics of the *Pnma* cell. From our unpublished data on the related charge ordered system $Y_{0.5}Ca_{0.5}MnO_3$ of pronounced orthorhombicity we concluded, however, that the Mn^{4+} spins were inclined to the same extent, keeping spins in the

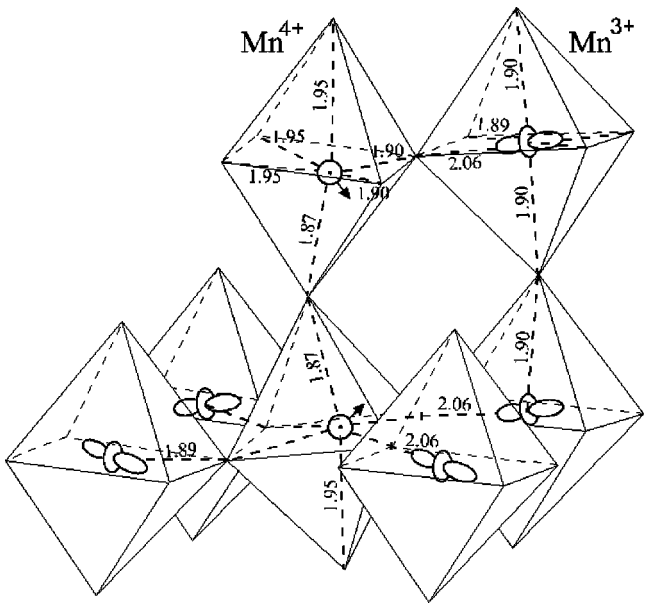

FIG. 2. The charge and orbital ordering in $Pr_{0.5}Ca_{0.09}Sr_{0.41}MnO_3$. Note the correlation of the off-center shifts along the Mn^{4+} chains (*b* axis in the *Imma* cell). In neighboring chains, the shifts are opposite so that the structure remains centrosymmetric. There are, however, indications that in some defective systems the arrangement is changed to a noncentrosymmetric one.

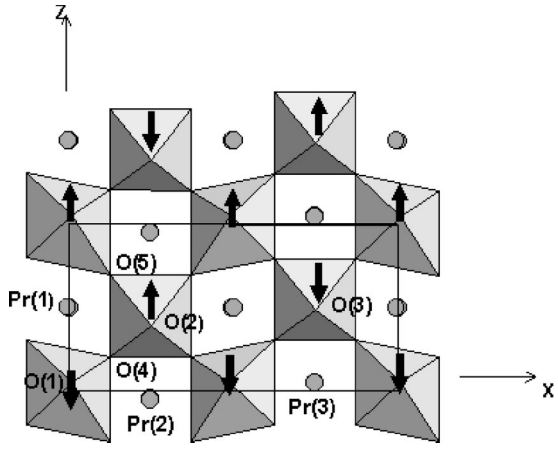

FIG. 3. The (010) layer of the low-temperature structure in $Pr_{0.5}Ca_{0.09}Sr_{0.41}MnO_3$ and the orientation of manganese moments. Tetragonal distortion of the $Mn^{3+}O_6$ octahedra is exaggerated in order to emphasize the structural modulation. The arrangement of distortions in the next layer is analogous, the moments are reversed.

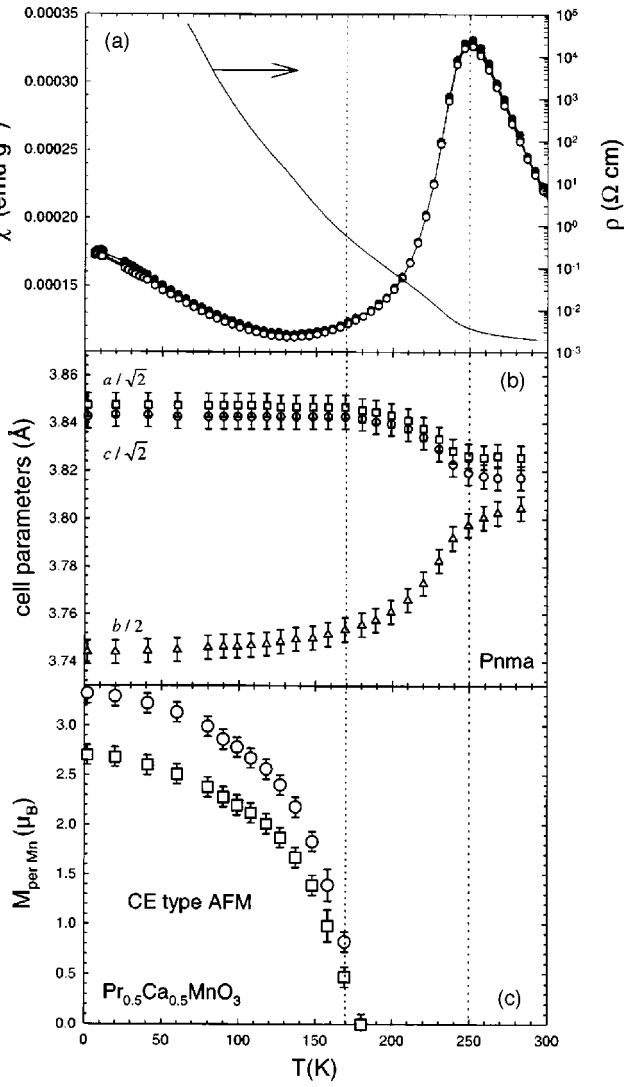

FIG. 4. $Pr_{0.5}Ca_{0.5}MnO_3$: temperature dependence of (a) the susceptibility (left axis), the resistivity (right axis), (b) the lattice parameters, and (c) the antiferromagnetic components. The dotted lines delimit the antiferromagnetism and the charge ordered state.

Mn^{3+} and Mn^{4+} sublattices parallel.

Despite the overall fit with the observed diffraction pattern ($\chi^2 = 1.87$), it should be noted that the discommensuration model failed in predicting of the asymmetrical broaden-

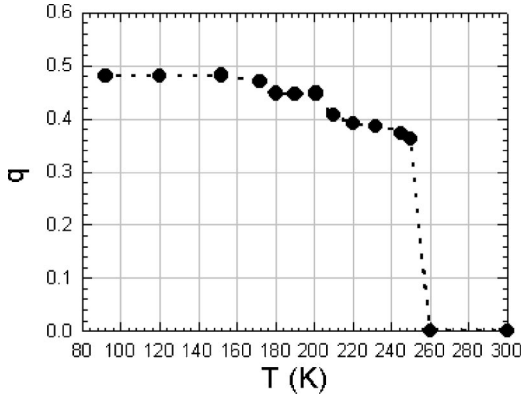

FIG. 5. The modulation vector $\vec{q} = 1/2\text{-}\varepsilon,0,0$ in $Pr_{0.5}Ca_{0.5}MnO_3$ upon sample heating (electron-diffraction data).

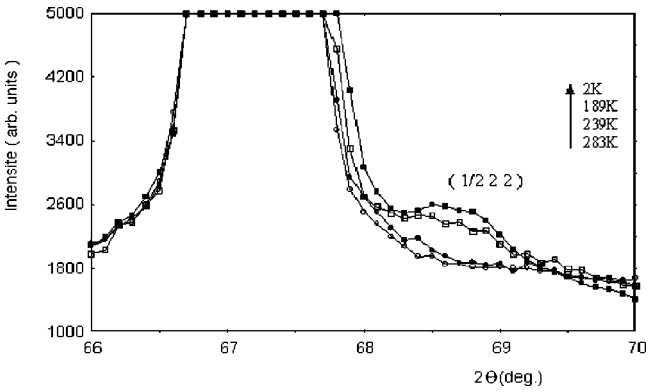

FIG. 6. Temperature evolution of the main superstructure line (1/2,2,2), characteristic for charge ordering in $Pr_{0.5}Ca_{0.5}MnO_3$ (neutron diffractometer G41).

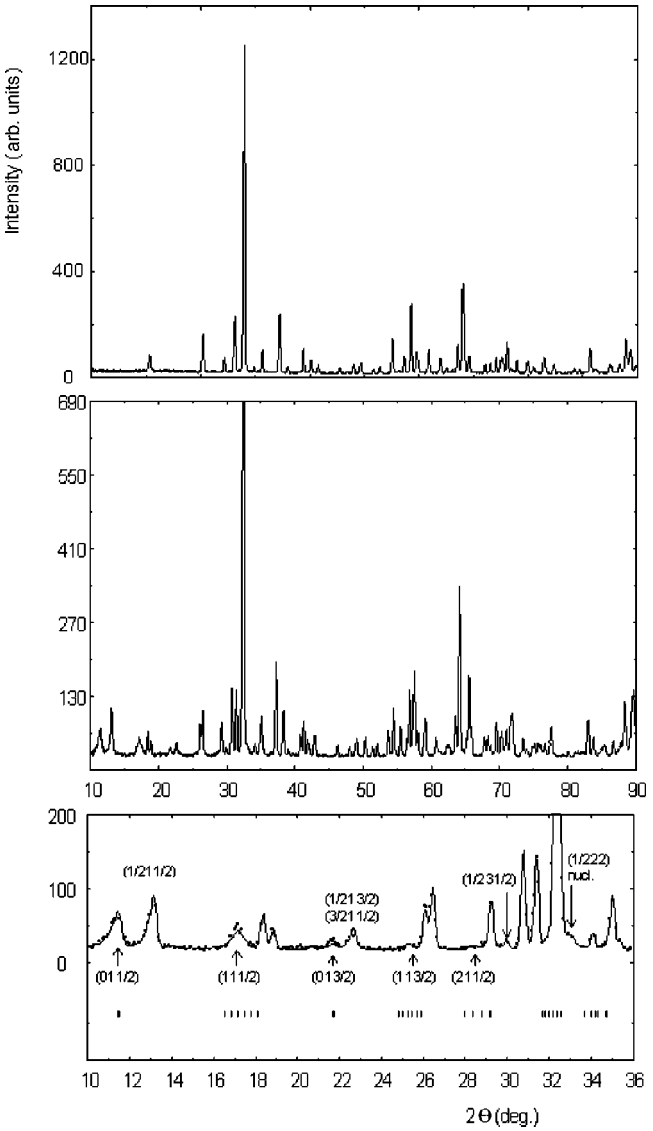

FIG. 7. The high-resolution neutron-diffraction patterns of $Pr_{0.5}Ca_{0.5}MnO_3$ at 292 and 10 K. The lower panel shows the observed and calculated profiles in low 2θ region. Due to incommensurity, the magnetic lines from Mn^{3+} sublattice are, in fact, composed of satellites in positions shown by ticks.

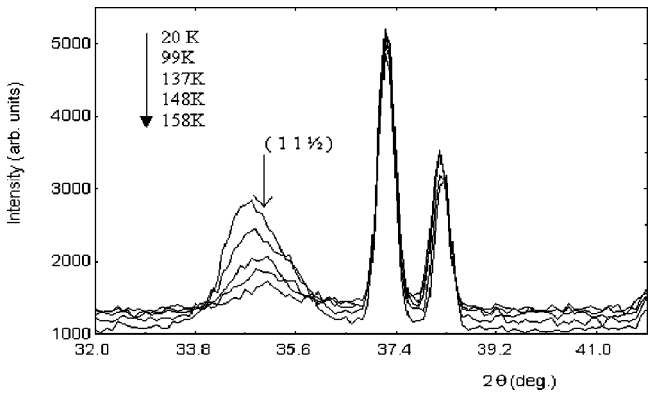

FIG. 8. Asymmetrical broadening of the magnetic line (1,1,1/2) in dependence on temperature (neutron diffractometer G41).

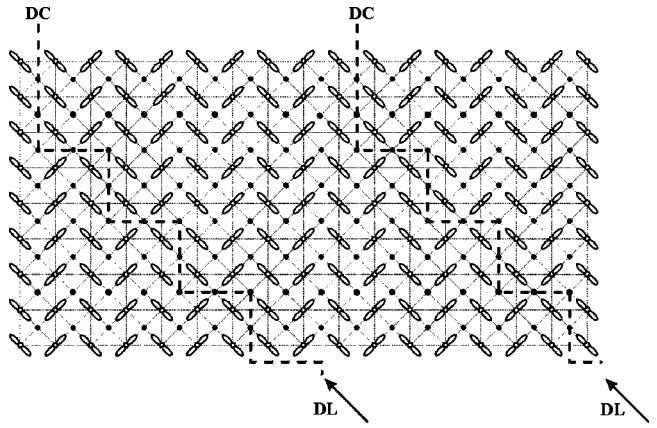

FIG. 9. Two kinds of orbital ordering defects responsible for the incommensurate modulation in the Mn^{3+}/Mn^{4+}(1:1) perovskites—discommensurations (DC) and dislocations (DL). Schematic view of one perovskite layer depicts a perfect valence order of Mn^{3+} (open circles) and Mn^{4+} (closed circles). The heavy-dashed lines represent boundaries where regular alternation of polarized e_g orbitals shown by the lobes is violated. The steplike course of dislocations reflects the fact that one of the orbital polarizations is preferred in the *Pnma* manganites.

ing of some less intense magnetic peaks of the Mn^{3+} set. The discrepancy could be removed considering additional defects of the orbital order that we call *dislocations*. They are schematically illustrated together with the above-mentioned discommensurations in Fig. 9. At this moment the dislocations are rather hypothetical but they are closely related to structures that were already observed by lattice imaging in some charge ordered manganites with oblique modulation vector.[8] Indeed, the arrangement in lower part of Fig. 9 would correspond to $\vec{q}=1/2\text{-}\varepsilon,0,\varepsilon$ if there were a long-range order. An interesting feature is orientation of the $d_{3z^2-r^2}$ orbitals along the dislocation lines, which reminds orbital polarization in the *C*-type antiferromagnets like $Pr_{0.2}Ca_{0.8}MnO_3$.[9] We assume that by reversal of neighboring orbitals the *C*-type arrangement grows into length and breadth. The growth of the dislocation lines causes the discommensurations to move and thus enables the temperature change of incommensurity. As another important consequence we mention that the *C*-type orbital arrangement brings about a strong tendency of spins to align in the direction of dislocations. In this way the observed inclination of moments from the *c* axis in the charge ordered systems with incommensurate modulation can be understood.

IV. DISCUSSION

The $Pr_{0.5}Ca_xSr_{0.5-x}MnO_3$ samples with $x=0.09$ and 0.5 are the extreme compositions for occurrence of the charge and orbital order in that series. In the first compound, such state is achieved from the high-temperature ferromagnetic phase by a first-order transition at which the tilt pattern is changed. The most important result of the present neutron- and electron-diffraction study is the complete structural determination of the Mn^{3+}/Mn^{4+} superstructure. On the other hand, the investigation of the $Pr_{0.5}Ca_{0.5}MnO_3$ compound that shows gradual evolution of the ordering may shed light onto dynamic correlations that precede the static orbital arrangements.

It is generally accepted that cation valences can be deduced by a bond valence summation based on experimental interatomic distances. Let us first discuss the Mn-O lengths observed at the absence of charge order in $Pr_{0.5}Ca_xSr_{0.5-x}MnO_3$ and some other manganites. The data are summarized in Table. II. The bond valence sums (BVS) were calculated using standard expression and empirical parameters tabulated in Ref. 10. A correction for thermal expansion was applied if appropriate. It appears that the BVS work exceptionally well for the pure Mn^{3+} or Mn^{4+} perovskites while for compounds with formal $Mn^{3.5+}$ valence the summation leads to a clear overestimation. The deviation seems to be larger for the strontium-rich samples, irrespec-

TABLE II. The Mn-O distances and calculated bond valence sums in perovskite manganites.

Compound	$PrMnO_3$[a] Ref. 7	$CaMnO_3$ Ref. 11	$La_{0.5}Ca_{0.5}MnO_3$ Ref. 6	$Pr_{0.5}Ca_{0.5}MnO_3$	$Pr_{0.5}Ca_{0.09}Sr_{0.41}MnO_3$ Ref. 4		$Pr_{0.5}Sr_{0.5}MnO_3$ Ref. 3
Temperature(K)	292	292	292	292	292	200	292 10
Space group	*Pnma*	*Pnma*	*Pnma*	*Pnma*	*Imma*	*I*4/*mcm*	*I*4/*mcm Fmmm*
Mn-O distances	1.92	1.895	1.941	1.937	1.928	1.925	1.927 1.900
	1.96	1.900	1.944	1.944	1.938	1.925	1.927 1.941
	2.19	1.903	1.946	1.946	1.938	1.946	1.947 1.958
BVS	3.09	4.04	3.62	3.64	3.69	3.68	3.69 3.70

[a]4% Mn^{4+} in the sample by chemical analysis.

tive of whether the phase is metallic or insulating. We relate this observation to the size mismatch of Pr and Sr ions, which means possibly that the real Mn-O distances are somewhat larger than the refined ones.

As to the charge ordered phases, the calculation based on the $Pr_{0.5}Ca_{0.09}Sr_{0.41}MnO_3$ data at 10 K (for the Mn-O distances, see Fig. 2) gave an unexpectedly small difference of the BVS for Mn^{3+} and Mn^{4+} sites, which amounted to 3.83 and 3.58, respectively. For the other system under investigation, $Pr_{0.5}Ca_{0.5}MnO_3$, the constrained refinement allowed only a rough estimate of real distances. More significant data achieved by a combined neutron and x-ray diffraction on $La_{0.5}Ca_{0.5}MnO_3$ in Ref. 6 gave calculated BVS of 3.88 and 3.42, also apparently far from a complete Mn^{3+}/Mn^{4+} disproportion. On the other hand, the electron localization evidenced by the resistivity measurements, the importance of ideal $Mn^{3+}/Mn^{4+}(1:1)$ concentration in the charge ordering effects and other facts indicate that the charge disproportion does exist. We assume, therefore, that electron redistribution in the charge ordered phase involves also oxygen ligand states. Such e_g-$2p$ hybridization might be further reinforced with the off-center Mn^{4+} location.

With rather similar Mn-O distances observed for the two manganese sites, the elastic interactions appear to be less important in the $Mn^{3+}/Mn^{4+}(1:1)$ ordering and the idea promoted by Khomskii *et al.*[12] that the main energy gain is associated with electronic interactions seems to be justified. An important support to this assumption came recently from the *ab initio* calculation for $Pr_{1-y}Ca_yMnO_3$ by Anisimov *et al.*[13] who demonstrated that the exchange mechanism (caused by an interplay of the on-site Coulomb interaction and the intersite hopping) is able by itself to give a correct picture of the spin and orbital ordering, without taking Jahn-Teller distortions into account. We expect that also in the dynamic regime of the disordered phase the charge fluctuations are coupled with certain orbital correlations and give rise to lattice modes that may be active in the ordering process.

The present electron-microscopy experiments on $Pr_{0.5}Ca_{0.5}MnO_3$ have shown that the charge and orbital ordering originates and decays as an incommensurate configuration with wave vector $\vec{q}=1/2\text{-}\varepsilon,0,0$. The hypothetical soft lattice mode responsible for the modulated structure in $Pr_{0.5}Ca_{0.5}MnO_3$ is illustrated schematically in Fig. 10(a). It represents an e_g density (Jahn-Teller) wave[14] that is coupled with a displacive modulation of a transversal acoustic phonon type. Each manganese site oscillates from one fully polarized e_g orbital state (+) to its opposite (−), through some partially polarized and unpolarized states. Here, the (+) and (−) represent two eigenstates that may be either $d_{3z^2-r^2}$ and $d_{x^2-y^2}$ (associated with local Jahn-Teller distortions $\pm Q_3$), or linear combinations like $d_{3z^2-r^2}+d_{x^2-y^2}$ and $d_{3z^2-r^2}-d_{x^2-y^2}$ (associated with $\pm Q_2$). In the system of mixed Mn^{3+}/Mn^{4+} ions the orbitally polarized states can be interpreted as electron occupated, i.e., Mn^{3+} sites, whereas the unpolarized states refer to the Mn^{4+} sites. Since the situation in Fig. 10(a) shows instantaneous orbital correlations for the incommensurate wave vector $\vec{q}=1/2\text{-}\varepsilon,0,0$, it, in fact, depicts different stages of the e_g electron transfer between nearest manganese neighbors. In such way the soft mode

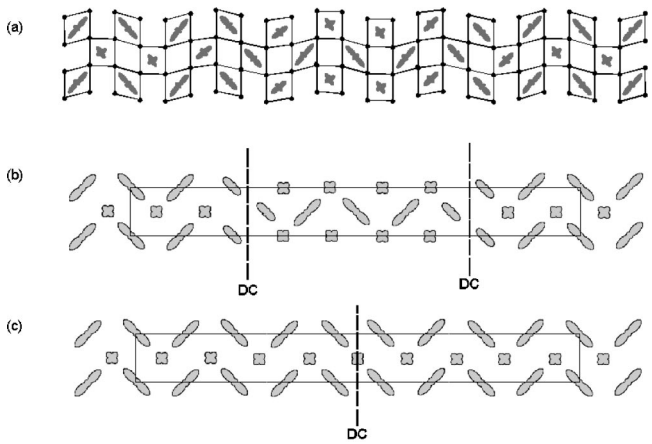

FIG. 10. The schematic view of possible arrangements of the e_g electron density in perovskites. The figure actually corresponds to $\vec{q}=1/2\text{-}\varepsilon,0,0$ with $\varepsilon=1/18\sim0.056$. In the homogeneous wave (a) the orbital polarization varies continuously and couples with displacive modulation of a transversal acoustic character, which is here depicted by distortions of the MnO_6 octahedra. The distorted waves (b) and (c) consist of domains of ideal $Mn^{3+}/Mn^{4+}(1:1)$ order separated by boundaries (discommensurations) at which the phase is changed to $\pi/2$ or π. The MnO_6 distortions or displacements (not shown) are arranged in the commensurate domains analogously to Fig. 3.

reflects the ideal $Mn^{3+}/Mn^{4+}(1:1)$ ratio, irrespective of the q value. The actual wave vector of the soft mode is possibly given by an energy equilibrium between the electronic interactions that prefer zone-boundary vector $q=1/2$ and the lattice vibrations of the acoustic type with minimum energy for the zone center $q\rightarrow0$.

Freezing of the soft mode is accompanied with valence localization and increase of the Jahn-Teller distortions. Both effects are strongly coupled to the lattice. McMillan[15] has shown that, in such cases, the homogeneous wave becomes disadvantageous. Instead, the domains of perfectly locked-in wave are formed, separated by discommensurations in which the phase of the wave is changed abruptly. For our case of $\vec{q}=1/2\text{-}\varepsilon,0,0$, the situation is shown schematically in Fig. 10(b) and 10(c). In the domains there is an ideal $Mn^{3+}/Mn^{4+}(1:1)$ order in which two orbital polarizations on the Mn^{3+} sites alternate regularly. Two different defects are shown, with phase shift $\pi/2$ and π, which can act as discommensuration boundaries. There are strong arguments that immediately below T_{co} the $\pi/2$-type discommensurations are first formed. It is evidenced by the fact that in the present $Mn^{3+}Mn^{4+}(1:1)$ system the incommensurate modulation starts with $q\sim1/3$ which means necessarily a $\pi/2$-type arrangement (see, e.g., the charge and orbital ordering in $La_{0.33}Ca_{0.67}MnO_3$ recently determined.[16]) The type of discommensurations becomes uncertain in the intermediate region between T_{co} and T_N where the system develops towards the ideal order with $q\sim1/2$. Below T_N, the discommensurations are exclusively of the π type, which is evident from the broadened Mn^{3+} and sharp Mn^{4+} magnetic lines in neutron-diffraction patterns. The suppression of the $\pi/2$-type discommensurations is probably of the same electronic origin as the orbital ordering itself—such defects would impose magnetic frustration.

We suggest that the discommensurations may move in the course of temperature by a dislocation process. Their instantaneous location is, however, not arbitrary. Considering that two e_g orbital states, polarized along directions [101] and $[10\bar{1}]$, respectively, are nonequivalent in the *Pnma* perovskites, it seems advantageous if the e_g orbitals at each site of the discommensuration boundary are polarized along the more suitable diagonal direction and the number of Mn^{3+} sites in the commensurate domain is even, as actually shown in Fig. 10(c). (The character of dislocation lines shown in Fig. 9 follows the same reasoning). When the discommensurations become more dense at the heating above T_N, one can imagine that they slid over multiples of $2a$. In this way the modulation vector $\vec{q}=1/2\text{-}\varepsilon,0,0$ is changed and acquires ''magical'' values $\varepsilon=1/(4n+2)\sim\cdots,0.033,0.038,0.045,0.056,0.071,0.100,0.167$. Such behavior is supported by the steplike temperature course of the modulation vector shown in Fig. 5.

V. CONCLUSIONS

The charge and orbital ordering in the series $Pr_{0.5}Ca_xSr_{0.5-x}MnO_3$ proceeds in different ways at the calcium- and strontium-rich sides. The ordering in $Pr_{0.5}Ca_{0.5}MnO_3$ arises in the paramagnetic phase of *Pnma* symmetry and develops through a sequence of modulated configurations between $T_{co}=250$ K and the CE antiferromanetic temperature $T_N=170$ K. At the cooling, the wave vector of the modulation is changed in increments and gradually approaches the commensurate value. Asymmetrical broadening of some magnetic lines in neutron-diffraction patterns and the inclination of Mn^{3+} and Mn^{4+} spins from principal axis show that the actual arrangement below T_N consists of domains of ideal (commensurate) order that are quasiperiodically separated by orbital defects–*discommensurations* and/or *dislocations*. Their experimentally determined spacing is about 170 Å. The presence of such defects does not necessarily mean a departure of the sample stoichiometry from the ideal 1:1 Mn^{3+}/Mn^{4+} ratio. Nevertheless, in case of small Mn^{4+} excess the local orbital arrangement (C type) at discommensuration boundaries and dislocations makes them suitable for trapping extra hole carriers.

The second compound, $Pr_{0.5}Ca_{0.09}Sr_{0.41}MnO_3$, is ferromagnetic below $T_C=240$ K and exhibits a sharp transition to the charge ordered state and CE antiferromagnetism at $T_{co}=T_N=180$ K. The low-temperature phase is completely long-range ordered and strictly commensurate. Based on the neutron-diffraction data, an unconstrained structural refinement was possible. Two distorted manganese sites were found—Mn^{3+} in a tetragonally elongated octahedron and Mn^{4+} located off center of the otherwise nearly regular octahedron. Although the insulating state and other properties of the charge ordered systems indicate entire charge disproportion of the Mn^{3+} and Mn^{4+} sites, the bond valence summation using observed Mn-O distances revealed the difference of only 0.25 electron. We link this discrepancy to highly asymmetrical electron distribution on oxygen atoms connecting the Mn^{3+} and Mn^{4+} sites, which is not properly accounted in a standard calculation of the bond valence sums.

ACKNOWLEDGMENTS

One of us (Z.J.) acknowledges financial support of the Grant Agency of Czech Republic (Grant No. 202/99/0413) and of CNRS, France (PICS No.280).

[1] F. Damay, C. Martin, A. Maignan, M. Hervieu, B. Raveau, Z. Jirák, G. André, and F. Bourée, Chem. Mater. **11**, 536 (1999).
[2] A. Urushibara, Y. Moritomo, T. Arima, A. Asamitsu, G. Kido, and Y. Tokura, Phys. Rev. B **51**, 14 103 (1995).
[3] F. Damay, C. Martin, M. Hervieu, C. Martin, A. Maignan, B. Raveau, G. André, and F. Bourée, J. Magn. Magn. Mater. **184**, 71 (1998).
[4] F. Damay, Z. Jirák, M. Hervieu, C. Martin, A. Maignan, B. Raveau, G. André, and F. Bourée, J. Magn. Magn. Mater. **190**, 221 (1998).
[5] S. Krupička, M. Maryško, Z. Jirák, and J. Hejtmánek, J. Magn. Magn. Mater. **206**, 45 (1999).
[6] P.G. Radaelli, D.E. Cox, M. Marezio, and S-W. Cheong, Phys. Rev. B **55**, 3015 (1997).
[7] Z. Jirák, J. Hejtmánek, K. Knížek, and R. Sonntag, J. Solid State Chem. **132**, 98 (1997).
[8] C. Martin, A. Maignan, F. Damay, M. Hervieu, B. Raveau, Z. Jirák, G. André, and F. Bourée, J. Magn. Magn. Mater. **202**, 11 (1999).
[9] Z. Jirák, S. Krupička, Z. Šimša, M. Dlouhá, and S. Vratislav, J. Magn. Magn. Mater. **53**, 153 (1985).
[10] I.D. Brown, Acta Crystallogr., Sect. B: Struct. Sci. **41**, 244 (1985).
[11] K.R. Poeppelmeier, M.E. Leonowicz, J.C. Scanlon, J.M. Longo, and W.B. Yelon, J. Solid State Chem. **45**, 71 (1982).
[12] K.I. Kugel and D.I. Khomskii, Usp. Fiz. Nauk. **136**, 621 (1982) [Sov. Phys. Usp. **25**, 231 (1982)]; D.I. Khomskii and G.A. Sawatzky, Solid State Commun. **102**, 87 (1997).
[13] V.I. Anisimov, I.S. Elfimov, M.A. Korotin, and K. Terakura, Phys. Rev. B **55**, 15 494 (1997).
[14] Z. Jirák, Phys. Rev. B **35**, 5437 (1987); **46**, 8725 (1992).
[15] W.L. McMillan, Phys. Rev. B **14**, 1496 (1976).
[16] M.T. Fernández-Díaz, J.L. Martínez, J.M. Alonso, and E. Herrero, Phys. Rev. B **59**, 1277 (1999); P.G. Radaelli, D.E. Cox, L. Capogna, S-W. Cheong, and M. Marezio, *ibid.* **59**, 14 440 (1999).